ISSN 0001-4338, Izvestiya, Atmospheric and Oceanic Physics, 2009, Vol. 45, No. 6, pp. 779–790. © Pleiades Publishing, Ltd., 2009.
Original Russian Text © V.G. Bondur, Yu.V. Grebenyuk, E.V. Ezhova, V.I. Kazakov, D.A. Sergeev, I.A. Soustova, Yu.I. Troitskaya, 2009, published in Izvestiya AN. Fizika Atmosfery i Okeana, 2009, Vol. 45, No. 6, pp. 833–845.

Surface Manifestations of Internal Waves Investigated by a Subsurface Buoyant Jet: 1. The Mechanism of Internal-Wave Generation

V. G. Bondur[a], Yu. V. Grebenyuk[a], E. V. Ezhova[b], V. I. Kazakov[b], D. A. Sergeev[b], I. A. Soustova[b], and Yu. I. Troitskaya[b]

[a] *Aerokosmos Scientific Center of Aerospace Monitoring, Gorokhovskii per. 4, Moscow, 105064 Russia*
e-mail: office@aerocosmos.info

[b] *Institute of Applied Physics, Russian Academy of Sciences, ul. Ul'yanova 46, Nizhni Novgorod, 603950 Russia*
e-mail: yuliya@hydro.appl.sci-nnov.ru

Received January 28, 2009; in final form, March 16, 2009

Abstract—In a large test reservoir with artificial temperature stratification at the Institute of Applied Physics, Russian Academy of Sciences, we have performed a major laboratory simulation of the nonstationary dynamics of buoyant turbulent jets generated by wastewater flows from underwater collector diffusers. The interaction of buoyant jets with the pycnocline leads to an active generation of internal waves. An analysis of the dependence of wave amplitude on the control parameter proportional to the rate of liquid flow from the collector diffuser has indicated that this dependence is adequately described by a function that is characteristic for the presence in the Hopf bifurcation system, which occurs for a soft actuation mode of self-oscillations of the globally instable mode. To check the conditions for the actuation of the globally instable mode, we have performed an auxiliary experiment in a small reservoir with a salt stratification formulated similar to the experiment in the big reservoir. Using the particle image velocimetry (PIV) method, we have measured the velocity field in the buoyant jet and constructed the profiles of transverse velocity in several sections. When the jet approaches the pycnocline, a counterflow is generated at the edges. A stability analysis for the resulting profiles of flow velocities performed by the method of normal modes has revealed that, for the jet portions with counterflow, the condition of absolute instability by the Briggs criterion for axisymmetric jet oscillations is satisfied, which testifies to the fact that the globally instable mode is actuated. The estimates for oscillation frequencies of the globally instable mode are well consistent quantitatively with the measured spectrum of jet oscillations.

DOI: 10.1134/S0001433809060115

1. INTRODUCTION

A key source of pollution of coastal water areas is waste-water disposal of [1]. This affects the general mass-exchange, hydrodynamics, and state of ecosystems of these water areas. There has been considerable recent interest in using aerospace methods for monitoring the zones of underwater collectors [1–4]. To assess the efficiency of remote methods, it is necessary to clarify the physical nature of disturbances caused by underwater disposal systems, as well to assess the possibility of their manifestations on the sea surface and registration by remote methods. Currently the physical mechanisms that can cause surface manifestations of deep sinks are not clearly understood. The physical mechanisms of the formation and propagation of turbulent jets in stratified water media of coastal water areas were considered in [5, 6]. In addition to the direct rise of disposed wastewater to the surface, some mechanisms conditioned by the surface deformation by buoyant vortices or internal waves and are proposed in [1, 3] and the surface manifestations of underwater sinks are explained by a complex interaction between turbulence, internal waves, tidal currents, and bottom topography in [4]. In this paper we discuss a mechanism of surface manifestations of underwater sinks that is related to the radiation of internal waves.

The typical diffuser of the modern disposal system is a collector with small vents allowing waters that have become almost freshwaters after being processed by waste disposal systems to flow into the saline oceanic water [7]. Turbulent jets flow out of these vents with a density smaller than the density of the ambient liquid. Here, buoyant plumes of disposal waters are generated. In this paper we propose a physical mechanism of the radiation of internal waves by underwater sinks, investigate the structure of the field of internal waves, and estimate the parameters of currents induced by these internal waves and the possible contrasts in the field of surface waves. This study consists of three sections. The mechanism of internal-wave generation by underwater sinks is proposed and investigated in the first part, the second part addresses the structure of internal waves radiated by these sinks, and the third part considers the problem of surface

manifestations of internal waves radiated by these sinks.

This paper describes the first part of the study; here, the hydrodynamic processes near an underwater collector are investigated on the basis of a major laboratory simulation. The main objective is to study the possibility of actuating internal waves by deepwater sinks and the efficiency of this mechanism. It should be noted that an indication that the internal waves can be radiated by buoyant jets is found in Turner's study [8]. Like in [3, 5, 6], this study presents experimental data indicating that the height of maximum rise of buoyant jets can be subjected to essential oscillations. In turn, this can lead to actuated internal waves. A similar phenomenon is described in the works by Karlikov et al. [9, 10], which show that, for a certain choice of current parameters, the fountain flowing from the below-surface water area makes oscillations that are accompanied by the actuation of surface waves. In [5, 6], the results of model calculations of the buoyant jets of deepwater sinks in a stratified medium are considered and compared with field measurement data.

In experimental studies [11–13], the oscillations of buried fountains observed in both turbulent [11, 12] and laminar regimes [13] are described.

In the first part of our study, we calculate the current and stratification parameters, ensuring that the conditions of major laboratory simulations of wastewater flow from the underwater collector are satisfied. We describe the laboratory setup, measuring apparatus, and experimental setup in the large thermally stratified test reservoir (LTSR) at the Institute of Applied Physics, Russian Academy of Sciences. The results of experiments performed in this reservoir are discussed. Also, an experiment performed in a smaller reservoir with a salt stratification is described and the use of the particle image elocimetry (PIV) technique for the profile of average jet velocity is discussed. We describe the theoretical calculations of self-oscillations in spatial currents when a counterflow is present and compare their results with experimental data.

2. MAJOR LABORATORY SIMULATION OF WASTEWATER FLOW FROM AN UNDERWATER COLLECTOR

By definition, the laboratory simulation of oceanic currents (in our case, turbulent buoyant jets flowing from an underwater collector) requires that the dimensionless parameters describing it in natural conditions coincide with the corresponding laboratory parameters and there should be a geometric similarity between them. To determine the parameters of a major simulation, we consider the main equations describing the evolution of integral parameters of buoyant turbulent jets of a round section in the stratified liquid obtained in [14] with the help of the following suppositions:

(1) the liquid is incompressible;

(2) the variations in the liquid density are smaller than its undisturbed value;

(3) the Reynolds number of the jet current is large, so that the molecular transport of mass and momentum is smaller than the turbulent transport;

(4) the turbulent transport along the jet current is smaller than the convective transport;

(5) the pressure in liquid is described by the hydrostatic relation;

(6) the jet radius is smaller than its radius of curvature;

(7) the velocity profile in the jet is approximated by the Gauss function

$$u^*(s, r, \varphi) = u(s)\exp\left(-\frac{r^2}{b^2}\right),$$

where s is the coordinate along the jet axis, r is the radial coordinate, φ is the angle between the xz plane and the given radius–vector, $u(s)$ is the velocity along the jet axis, and b is the jet radius;

(8) the profile of the jet density defect is also described by the Gauss function

$$\frac{\rho_a^*(s, r, \phi) - \rho^*(s, r, \phi)}{\rho_0} = \frac{\rho_a(z) - \rho(s)}{\rho_a(z_0)}\exp\left\{-\frac{r^2}{\lambda^2 b^2}\right\},$$

where ρ_a is the density of the environment, z_0 is the depth of the collector location, $\rho_a(z_0) = \rho_0$ is the density of ambient liquid at the collector level, $\rho(s)$ is the density along the jet axis, $\lambda = 1.16$ is a constant obtained from experimental data for the circular cross section of the jet [14];

(9) the law of entrainment is given by the relation

$$\frac{dQ}{ds} = 2\alpha\pi ub,$$

where Q is the volume flow through the jet cross section and $\alpha = 0.057$ is the turbulent entrainment coefficient.

The system of equations describing the integral parameters of this jet involves the following equations:

(i) the equation of jet flow change through entrainment

$$\frac{d}{ds}(ub^2) = 2\alpha ub; \quad (1)$$

(ii) the law of conservation of flow along the jet of the horizontal component of momentum

$$\frac{d}{ds}(u^2 b^2 \cos\Theta) = 0, \quad (2)$$

where Θ is the angle of jet slope to the horizon;

(iii) the law of change of the current along the jet of the vertical component of momentum through the buoyancy forces

$$\frac{d}{ds}(u^2b^2\sin\Theta) = 2g\lambda^2b^2\frac{\rho_a(z)-\rho(s)}{\rho_a(z_0)}; \quad (3)$$

(iv) the law of change of the buoyancy flux along the jet through the entrainment of the ambient nonuniformly distributed liquid

$$\frac{d}{ds}[ub^2(\rho_a(z)-\rho(s))] = \frac{1+\lambda^2}{\lambda^2}b^2u\frac{d\rho_a}{dz}\frac{dz}{ds}. \quad (4)$$

System (1–4) must be coupled by geometric relations linking the coordinate along the jet s and the angle of jet slope to the horizon Θ with the Cartesian coordinates x and y:

$$\frac{dx}{ds} = \cos\Theta, \quad (5)$$

$$\frac{dz}{ds} = \sin\Theta. \quad (6)$$

Let us introduce a new variable $\beta = g\left(\frac{\rho_a(z)-\rho(s)}{\rho_0}\right)$, and call it buoyancy. Then, Eqs. (3) and (4) can be rewritten as

$$\frac{d}{ds}(u^2b^2\sin\Theta) = 2\lambda^2b^2\beta, \quad (7)$$

$$\frac{d}{ds}(ub^2\beta) = -\left(\frac{1+\lambda^2}{\lambda^2}\right)ub^2N^2(z/h)\sin\Theta, \quad (8)$$

where $N^2(z/h)$ is the profile of the squared buoyancy frequency, which can be represented as $N^2(z/h) = N_0^2n^2(z/h)$, where h is the characteristic thickness of the pycnocline, N_0 is the value of buoyancy frequency, and $n^2(z/h)$ is a dimensionless function.

The initial conditions for the system are specified by the parameters of jet current at the point of flowing out from the collector:

$u=U_0$, $b=b_0$, $\Delta\rho=\Delta\rho_0$ ($\beta=\beta_0$), $\Theta=0$, $z=z_0$, $x=0$.

Let us show (2.1)–(2.6) system in dimensionless variables

$$\tilde{s} = s/b_0, \quad \tilde{x} = x/b_0, \quad \tilde{z} = z/b_0, \quad B = b/b_0,$$

$$V = u/U_0, \quad \beta = \frac{g\Delta\rho_0}{\rho_0}\gamma.$$

$$\frac{d}{d\tilde{s}}(VB^2) = 2\alpha VB, \quad (9)$$

$$\frac{d}{d\tilde{s}}(V^2B^2\cos\Theta) = 0, \quad (10)$$

$$\frac{d}{d\tilde{s}}(V^2B^2\sin\Theta) = 2\lambda^2B^2\gamma Ri, \quad (11)$$

$$\frac{d}{d\tilde{s}}(VB^2\gamma) = -\left(\frac{1+\lambda^2}{\lambda^2}\right)VB^2n^2(\tilde{z}/\tilde{h})\sin\Theta(\mathrm{Str}), \quad (12)$$

$$\frac{d\tilde{x}}{d\tilde{s}} = \cos\Theta, \quad (13)$$

$$\frac{d\tilde{z}}{d\tilde{s}} = \sin\Theta. \quad (14)$$

At these norms, the initial conditions in this case take the form

$B=1$, $V=1$, $\gamma=1$, $\Theta=0$, $\tilde{x}=0$, $\tilde{z}=z_0/b_0$.

It can be seen that system (9)–(14) and the boundary conditions are determined by four dimensionless parameters:

(i) the parameter of background stratification

$$\mathrm{Str} = \frac{N_0^2b_0\rho_0}{g\Delta\rho_0}, \quad (15)$$

(ii) the global Richardson number of the jet current

$$\mathrm{Ri} = \frac{g\Delta\rho_0b_0}{\rho_0U_0^2}, \quad (16)$$

(iii) the dimensionless thickness of pycnocline

$$\tilde{h} = h/b_0, \quad (17)$$

(iv) the dimensionless depth of the collection position

$$\tilde{z}_0 = z_0/b_0. \quad (18)$$

In the model experiment, the background-stratification parameters, geometric dimensions of the model, and liquid flow rate were determined on the basis of modeling conditions with respect to the number Ri, Str, $\tilde{z}_0$, $\tilde{h}$, as well as the geometric similarity.

3. EXPERIMENTAL SETUP IN THE LTSR

The current near the collector of the disposal system has been simulated in the LTSR at the Institute of Applied Physics, Russian Academy of Sciences. The LTSR dimensions are as follows: 20 m in length, 4 m in width, and 2 m in depth [15]. The density stratification in the LTSR is generated through liquid heating and cooling with the help of heat exchangers installed along lateral boundaries of the reservoir walls [15]. This results in the formation of a nonuniform vertical distribution of temperature in the reservoir. Here we have performed two series of experiments differing in the depth of occurrence of the temperature jump (Fig. 1).

The general schematic of the experiment is shown in Fig. 2. The physical model of the collector is a

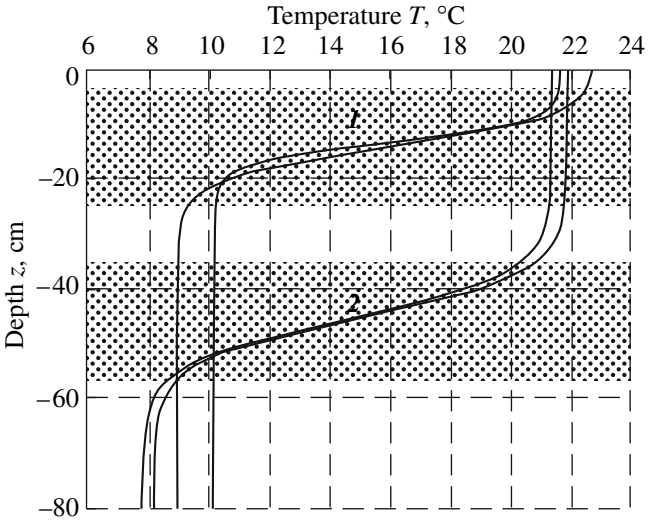

Fig. 1. Profiles of temperature stratification in the LTSR: operating profiles with (1) low thermocline, (2) deep thermocline.

metallic tube that is blocked at one end and has a length of 1.3 m and a diameter of 1.2 cm; the lateral surface of this tube includes 5 vents with a diameter of 3 mm located at a distance of 30 cm from one another at the same level. The rube is oriented horizontally across and in the middle of the reservoir at depth H from the surface (see Fig. 2). The vent axes are oriented horizontally. The collector model is connected by a hose through the free end with a tank filled with a solution of ethyl alcohol, the density of which during the experiments was kept constant and equal to 0.93 g/cm^3. The average rate of the solution flow out of vents in the collector model is determined through the solution consumption

$$V_0 = \frac{Q}{S_\Sigma} = \frac{V}{5S_0\Delta t},$$

where S_0 is the area of a single vent and Δt is the time needed for the control volume V of the solution to outflow.

The parameters characterizing the field and laboratory conditions

Parameter	Field conditions	Laboratory conditions
Diameter b_0 of vent in collector	8 cm	0.3 cm
Depth z_p from the middle of pycnocline to collector	30 m	110 cm
Pycnocline thickness h	5.5 m	20 cm
Distance l between collector vents	7 m	30 cm
Maximum value N_0^2 of buoyancy frequency	5×10^{-2} s^{-1}	0.45 s^{-1}
Initial difference $(\rho_1 - \rho_0)$ between densities of jet and ambient liquid	0.0235 g/cm^3	0.07 g/cm^3
Jet rate V_0 at the output of diffuser	3 m/s	1 m/s

The table shows the parameters of the current and stratification in the LTSR, which enable the typical conditions of the coastal area and characteristic parameters of the collector diffuser of the underwater disposal system to be simulated on a massive scale [3] with respect to the numbers Ri, Str, $\tilde{z}_0$, $\tilde{h}$ and a geometric similarity on the scale of 1 : 27. In this case, the Reynolds number at the vent output was around 3000, which ensures the developed turbulence mode of buoyant jets in the laboratory experiment. The distance from the middle of the thermocline to the surface constituted 40–50 cm (the maximum depth for the thermocline location reached in the LTSR) for the first series of experiments and 13–15 cm (the minimum depth for the thermocline location reached in the LTSR) for the second series.

The variation of the flow rate through the change in the tank-solution level during the experiment does not exceed 10% (the average value was 5%). In the LTSR, a temperature stratification of the thermocline type was created and its parameters were kept invariant in the course of all experiments. The total depth of the liquid filled in the reservoir constituted 162 cm and was constant during the experiments. The temperature oscillations in the environment caused by jet buoyancy were fixed with the help of an antenna of 13 temperature sensors (thermistors) measuring the values of water temperature in the range from 9 to 20°C with an error of no more than 0.05°C and a time constant of 0.3 s. The antenna was foxed on a special portable rack at different distances from the collector model. The analog signals from thermistors were transformed with the help of an analog-to-digital converter and recorded to the computer's hard disk. The flow-velocity profiles were measured by a three-component Doppler velocimeter installed immediately behind the antenna of temperature sensors on the scanning device.

Two series of experiments with different depths of the thermocline location, as well as a test series preceding the first one, were performed. The test series consisted of 14 experiments with varying rates of the liquid flowing from the collector diffuser (30, 40, 48, 55, 70, 80, 90, 95, 100, 105, 120, 125, 140, and 190 cm/s) for fixed stratification parameters (at a maximum buoyancy frequency of 0.45 s^{-1} and a distance of 40–50 cm

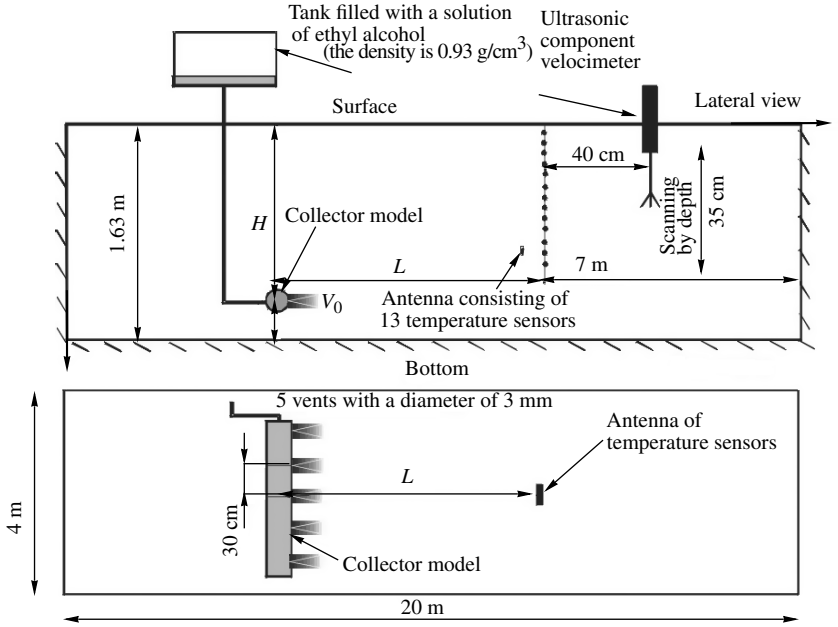

Fig. 2. General schematic of the experiment for simulating a current induced by the wastewater disposal system.

from the surface to the thermocline middle). The first series consists of 24 experiments for four velocity values (40, 70, 100, and 145 cm/s) for the same stratification. For each value, six experiments were performed. This involved 5 runs of 10 min and one run of 20 min. The second series consists of 16 experiments for the same four velocity values for the stratification with a low thermocline. In the second series of experiments, the velocity fields were measured on the reservoir surface by the method of Particle Tracing Velocimetry (PTV).

4. THE RESULTS OF THE EXPERIMENT IN THE LTSR

Using the measured temporal temperature cross sections and a special-purpose computer program, we calculated the average characteristics of the temperature field, depth of isotherm location, spectra of shifts of liquid particles relative to their equilibrium level, and dispersion of isotherm shifts. The shift dispersion of each isotherm was calculated by the formula

$$\langle \sigma_\eta^2 \rangle = \langle \eta^2 \rangle = \int_{f_{\min}}^{f_{\max}} Sp(f)df,$$

where $Sp(f)$ is the spectrum of isotherm shifts relative to the median level; the meaning of frequencies $f_{\max}$ and $f_{\min}$ will be described below.

Figures 3 and 4a show examples of temporal cross sections of the temperature field for a 100-cm/s liquid flow from the diffuser (for which the conditions of the major simulation are satisfied) for stratification with deep and low thermocline. The left sides of the figures show the isotherms corresponding to temperatures from 9 to 20°C for Fig. 3 (from 10 to 20°C for Fig. 4) with a step of 1°C, which was constructed by measurement data obtained by all sensors (the dashed lines mark 4 isotherms in the range of from 9 to 12°C in Fig. 3 and from 10 to 13°C in Fig. 4). It can be seen from the figures that the buoyant jet induces temperature oscillations (isotherm shifts).

Figures 3 and 4b show the spectra of isotherm shifts for the rate of liquid flow from the diffuser of 100 cm/s obtained by the ensemble averaging of six runs in the case of stratification with a deep thermocline and five runs for stratification with a low thermocline. The spectra include a clearly expressed peak in the range of frequencies from $f_{\min} = 0.02$ Hz to $f_{\max} = 0.05$ Hz, which are smaller than the maximum value of buoyancy frequency (which constituted 0.07 Hz (0.45 rad/s) in the given series of experiments). Thus, the frequency of oscillations induced by the buoyant jet is in the range of propagation of internal gravitational waves. Let us note that the values $f_{\min} = 0.02$ Hz and $f_{\max} = 0.05$ Hz were chosen for calculating the dispersion of isotherm oscillations.

Let us discuss the mechanism of actuation of the observed oscillations. First of all, we emphasize the key difference of this phenomenon from the spatial oscillations of buried jets [12], which can be described by the solution (oscillating with respect to $\tilde{s}$) of the stationary system of equations (9)–(14). In our experiments, when the buoyant jet interacts with the thermocline, a nonstationary process (oscillations with a peak at the frequency range) is observed.

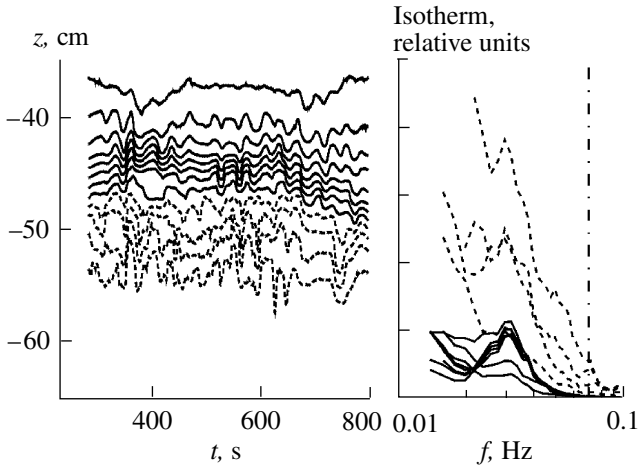

Fig. 3. Temporal cross sections of isotherm oscillations for the rate of liquid flow from the collector of $V_0 = 100$ cm/s in the mode of stratification with deep thermocline. The right side shows isotherm spectra; the dash-dotted lines indicate the maximum value of buoyancy frequency.

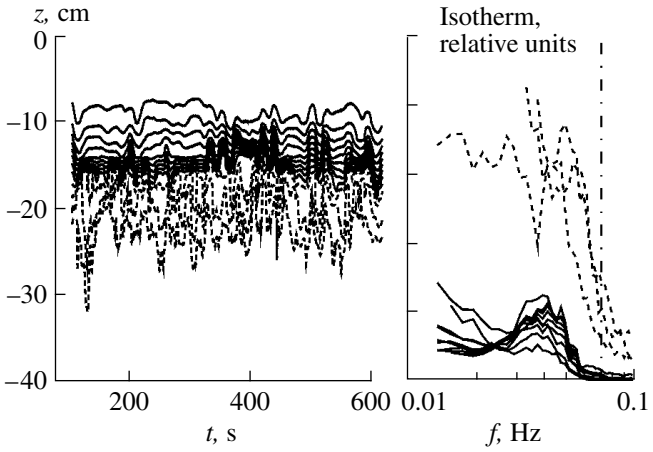

Fig. 4. Temporal cross sections of isotherm oscillations for the rate of liquid flow from the collector of $V_0 = 100$ cm/s in the mode of stratification with low thermocline. The right side shows isotherm spectra; the dash-dotted lines indicate the maximum value of buoyancy frequency.

A possible way for thermocline oscillations to emerge is by the evolution of hydrodynamic instability in the jet along the thermocline. However, in the given experiment, for a 100-cm/s liquid flow from the diffuser, the minimum gradient Richardson number of the jet was $\mathrm{Ri} = 0.43 > 0.25$. For this value of the Richardson number, according to the Miles–Howards criterion [16, 17], the current is stable.

To explain the nature of observed oscillations, we made a hypothesis on the actuation of self-oscillations in the system. It is known that, if the system has self-oscillations, their amplitude a satisfies the Landau equation [18]

$$\frac{da}{dt} = a(\mu(R - R_c) - \nu|a|^2), \tag{19}$$

where R is a control parameter, R_c is its critical value, and ν is a parameter of linear attenuation.

The parameters entering into Eq. (19) can be calculated if the approximation of weak linearity (for example, see [19]) is applicable. In addition, they can be found from an approximation of experimental data. In this case, the amplitude of steady-state oscillations satisfies the equation

$$\left((R - R_c) - \frac{\nu}{\mu}|a|^2\right)a = 0. \tag{20}$$

The control parameter is represented by the rate of liquid flow from the collector vents and $\langle\sigma_\eta^2\rangle = |a|^2/2$. Here, the parameters entering into Eq. (20) can be determined from the condition of the best approximation of the resulting experimental data.

We constructed experimental dependences for the average dispersion of isotherm shifts in the upper part of the thermocline (an averaging over isotherms 13–19°C in Fig. 5a for the first series of experiments and 14–20°C in Fig. 6a for the second series of experiments) and in the lower part of the thermocline (an averaging over isotherms 9–12°C in Fig. 5b for the first series of experiments and 10–13°C in Fig. 6b for the second series of experiments) on the rate of liquid flow from the collector model. The considerable scatter in the results obtained in different runs for one and the same flow rate can be explained by the fact that the jet current in the area of the sensor location is not two-dimensional (the jets did not completely merge together). It can be seen that the experimental data are well approximated by linear dependences following from Eq. (20). As was shown in [20], the existence of this dependence is a reliable criterion for the actuation of the globally instable mode.

It should be noted that a key criterion for the existence of the globally instable mode in the system is also assumed to be the narrow-band oscillation spectrum [20]. It can be seen from Figs. 3 and 4b that the spectra have a clearly expressed peak in the frequency range between $f_{\min} = 0.02$ Hz and $f_{\max} = 0.05$ Hz. This also speaks in favor of self-generation in the system.

In studying self-generation in the system, it is important to clarify the mechanism of emergent positive feedback. In the present experiment, we consider a system that is a jet where each cross section is homogenous in through turbulent mixing and which acquires a pulse due to the action of buoyancy forces; then it is captured by the pycnocline. The problem of positive feedback for self-oscillations in such a system is formally reduced to the study of conditions for the hydrodynamic stability of this current. Here, for exponentially growing self-oscillations of such a sys-

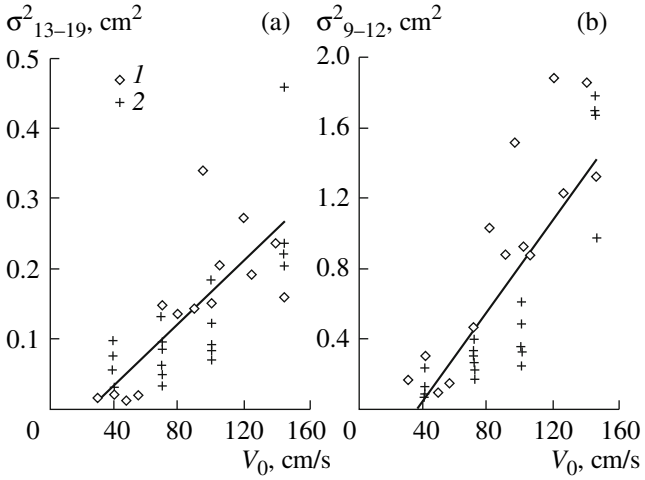

Fig. 5. Dependences of the average dispersions of flow-rate fluctuations in the mode stratification with deep thermocline: (a) for the upper part of the thermocline (an averaging over isotherms 13–19°C and (b) for the lower part of the thermocline (an averaging over isotherms 9–12°C). (*1*) The test series of experiments and (*2*) the first series of experiments.

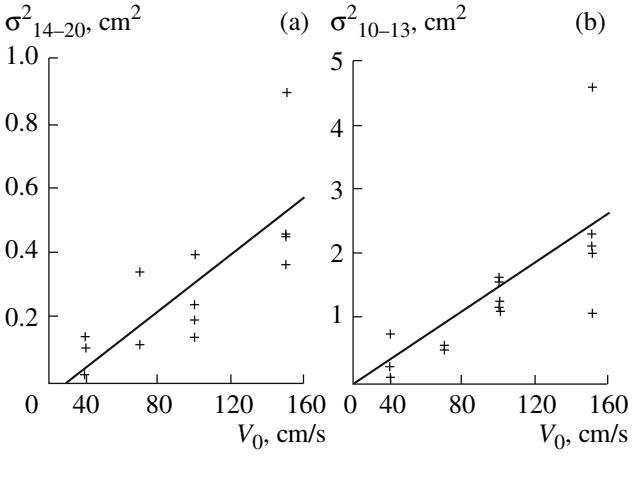

Fig. 6. Dependences of the average dispersions of flow-rate fluctuations in the mode stratification with low thermocline: (a) for the upper part of the thermocline (an averaging over isotherms 14–20°C and (b) for the lower part of the thermocline (an averaging over isotherms 10–13°C) in the second series of experiments.

tem, P. Monkewitz et al. [20, 21] introduced the conception of the globally instable mode. The exact solution of this problem is connected with large complexities and, apparently, can be obtained only with the help of direct numerical modeling. However, the feedback in the given system can be understood if one uses the approach developed in [20, 21], where it is proposed that the globally instable modes in current systems be described approximately. The buoyant jet is a typical example of such a system. These systems are characterized by the existence of a distributed feedback, the parameters of which are determined by some peculiarities of the flow field. For example, as is shown in [21], the positive feedback and globally instable modes caused by it are characteristic for jet currents with counterflow. To clarify the positive feedback in a buoyant jet captured by the pycnocline, we performed special experiments for studying the velocity field in the jet in the small reservoir with salt stratification by the PIV method.

5. DESCRIPTION OF THE EXPERIMENT IN A SMALL RESERVOIR WITH A SALT STRATIFICATION

To study the way that buoyant turbulent jets and ambient stratified liquid interact, we performed special experiments in the small reservoir. Here, a salt stratification of the pycnocline type is created. The distributions of density and buoyancy frequency are shown in Fig. 7. In this experiment, the collector model had only a single vent with a diameter of 1.2 mm that allowed freshwater to flow out with a rate of 50 cm/s. Here, the PIV method [22] was used. This digital method for investigating the velocity fields is based on a visualization of currents by additional tracers (particles). In this experiment, the particles were added into the freshwater liquid in the tank. The motion of particles was visualized by radiographing the jet with a vertical laser knife along the axis. The lateral view was recorded on a CCD-camera. The processing of the resulting video made it possible to obtain the velocity field in the laser-knife cross section at consecutive time points with a step of 0.25 s.

Figure 8 shows examples of measured instantaneous velocity fields. It can be clearly seen that the jets are retarded by stratification and propagate at the neutral buoyancy level, which is located on the lower boundary of the pycnocline.

The videotape recording also indicates that the upper boundary of the jet oscillates in the vertical plane; here, the oscillation spectrum has a clearly expressed peak at a frequency of 0.1 Hz (Fig. 9).

Figure 10 shows the instantaneous velocity profiles in different cross sections of the jet. To smooth the turbulent pulsations that arise on these profiles, averaging by the coordinate along the jet axis was performed. This includes the calculation of the mean profile of velocity on the basis of three adjacent profiles located 4.8 mm away from each another. It can be seen from this figure that the profiles have an almost flat front and there is a considerable counterflow in sections 2 and 3.

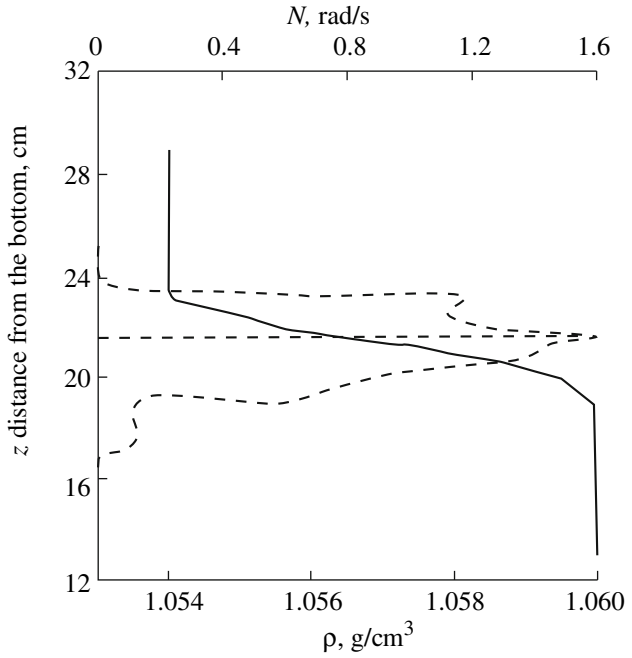

Fig. 7. Distributions of density and buoyancy frequency in the small reservoir.

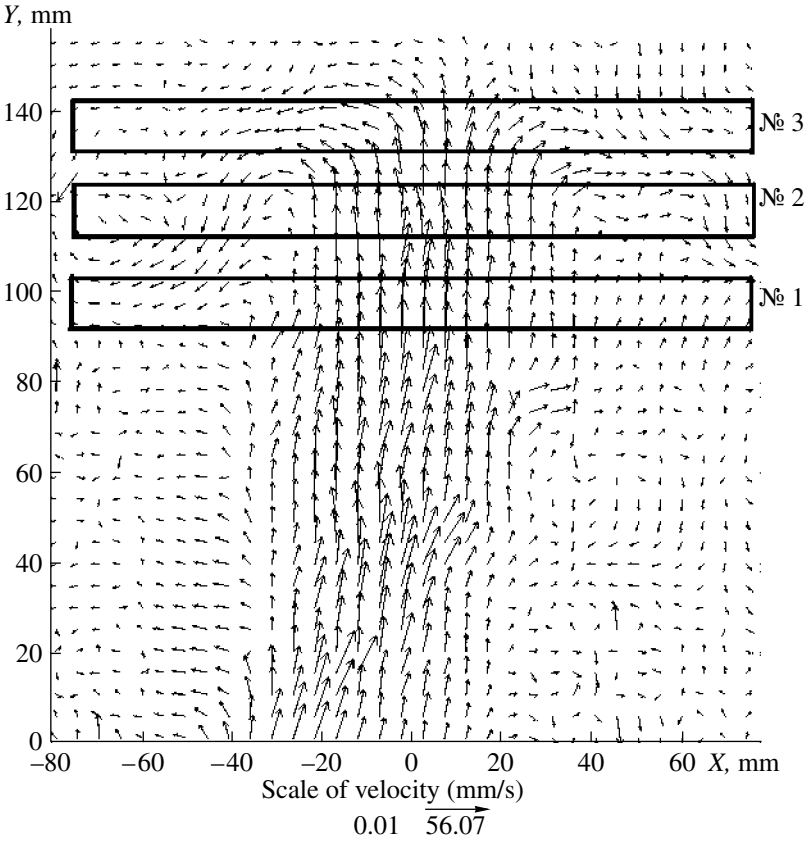

Fig. 8. Velocity field of buoyant turbulent jet.

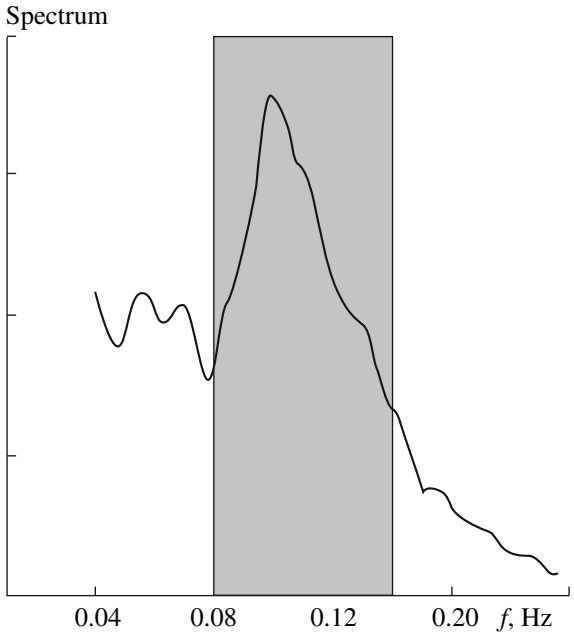

Fig. 9. Run and spectrum of oscillations of the upper boundary of the jet.

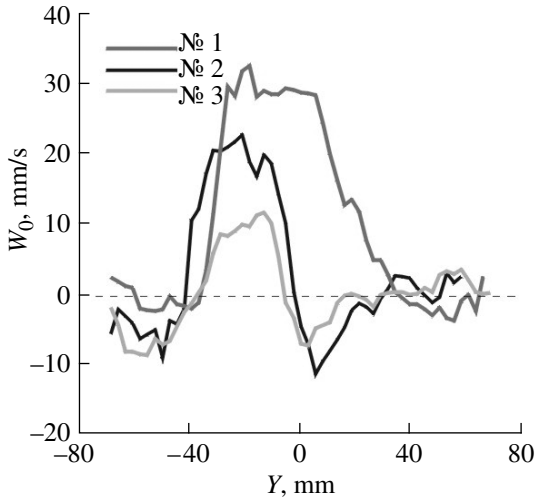

Fig. 10. Profiles of jet rate in cross sections *1*, *2*, and *3* (see Fig. 8).

6. THEORETICAL CALCULATION OF SELF-OSCILLATIONS IN SPATIAL JET CURRENTS

The phenomenon of actuation of self-oscillations in spatial jet currents was theoretically justified in studies by Huerre, Monkewitz, and Chomaz [20, 21, 23, 24]. In [20], the concept of local and global instability is introduced. The terms "local" and "global" refer to local instability of the profile of velocity and to the entire spatially inhomogeneous current, respectively.

Also in [20], a classification for spatial jet currents is introduced with respect to the type of instability: absolute and convective. The emergence absolute instability was shown to be affected by two factors: the presence of counterflow and the difference between the densities of the jet and the ambient liquid. In [24], the authors found that the availability of a finite range of instability along the direction of jet propagation is necessary for the existence of self-oscillations.

The counterflow can be easily seen on the velocity profiles in jets (Fig. 10), which may indicate the condition of the existence of the globally instable mode. Let us estimate its parameters.

The stability of nonparallel currents is normally analyzed in the following way: the current is divided into parts, each of which is taken to be quasi-parallel and treated by the method of normal modes. For each marked profile of the mean jet velocity, the dispersion relation $D(\omega, k; x)$ is obtained. Assuming that ω and k are complex, one can determine whether the given interval of a current is instable and the character of this instability. To determine the type of instability, the Briggs criterion [25] is used, which was developed for use in plasma physics and used in hydrodynamics for the first time in [20]. The criterion is formulated as follows. The form of local instability depends on the sign of the imaginary part of the absolute frequency $\omega_0 = \omega(k_0)$, where k_0 is determined from the relation $\frac{d\omega}{dk}(k_0) = 0$. The instability is absolute if $\mathrm{Im}\omega_0 > 0$ and convective otherwise. This criterion is supplemented with an additional requirement: the branching point ω_0 must appear as a result of the merging of two oppositely directed modes. Mathematically, this means that, for a sufficiently large $\mathrm{Im}\omega_0$, the branches $k^+(\omega)$ and $k^-(\omega)$ on the complex plain (Re k, Im k) must be located at opposite sides of the real axis Re k.

Let us note that the distributed positive feedback in a spatial current with the globally instable model is always connected with the existence of an interval of absolute hydrodynamic instability on this current. The Briggs criterion means that the existence of this interval is conditioned by the availability of two connected modes on the current: upstream and downstream. In this case, the upstream mode acquires energy from this interval through the resonance energy exchange, while the downstream mode delivers a positive feedback (the downstream transfer of pressure pulsations according to [20]). If the interval of absolute instability on a spatial current is finite, there are globally instable modes localized in the space because, by definition, the disturbances become broken by the current quicker than they grow in areas of convective instability.

In the calculations, the local profiles of velocity were approximated by a function of the form $W_0(r) =$

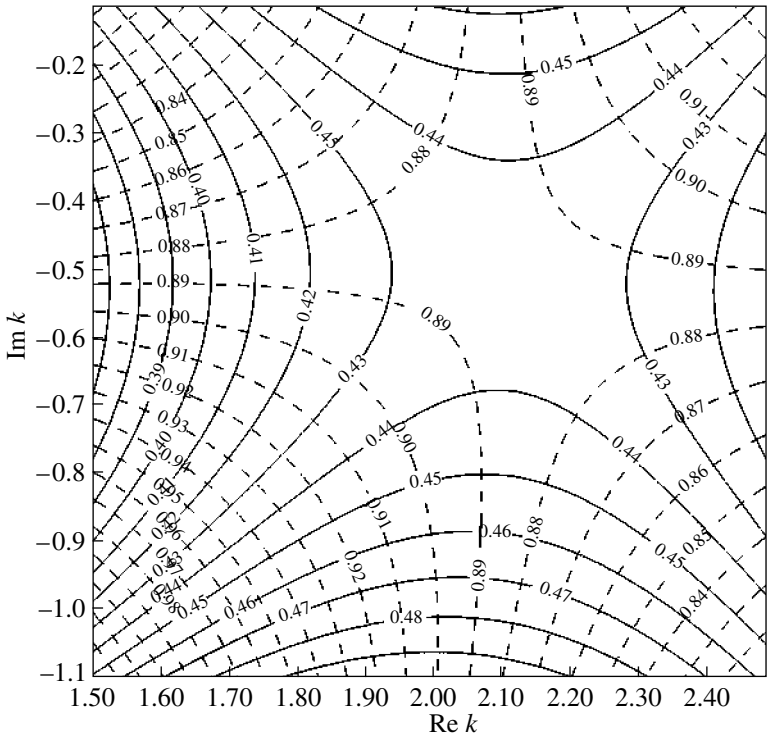

Fig. 11. An example of the form of curve levels Re ω(Re k, Im k) and Im ω(Re k, Im k) for one of the jet cross sections.

$\{\alpha \tanh[\beta(r-1)] + \gamma\}\exp(-\sigma r^6)$. Here, the parameters α, β, γ, and σ were chosen so that the local profile is matched by average (over a given cross section of the jet) values of the current, counterflow, and thickness. The dispersion relation was obtained from the solution of an eigenvalue problem for the analog of Rayleigh's equation for disturbances of an axisymmetric jet:

$$\frac{d^2p}{dr^2} + \frac{1}{r}\frac{dp}{dr} - \frac{2W_0'}{(W_0 - c)}\frac{dp}{dr} - k^2 p = 0$$

with the boundary conditions

$$p(0) = 1, \quad p(\infty) = 0.$$

In the calculations, the frequency ω and wave number k were assumed to be complex. The level curves of surfaces Re ω(Re k, Im k) and Im ω(Re k, Im k) were constructed with the help of the standard package Golden Software Surfer 32 (Fig. 11). We determined the position of the saddle point k_0 and the absolute frequency $\omega_0 = \omega(k_0)$.

Using this technique, we calculated the values of absolute frequencies for all experimentally measured profiles of average velocity. These calculations pointed to the existence of a finite interval along the jet propagation, where $\mathrm{Im}\,\omega_0 > 0$ is the area of absolute instability (Fig. 12).

It is difficult to make a detailed calculation of the frequency of self-oscillations in the given spatial current; however, as shown in [22], the frequency of these oscillations is close to Re ω_0. The calculations show that the real part of absolute frequency $\mathrm{Re}\, f_0 = \mathrm{Re}\dfrac{\omega_0}{2\pi}$ for different cross sections of the jet observed in the experiment varied in the range from 0.08 to 0.14 Hz. The range of calculated variations of the real part of

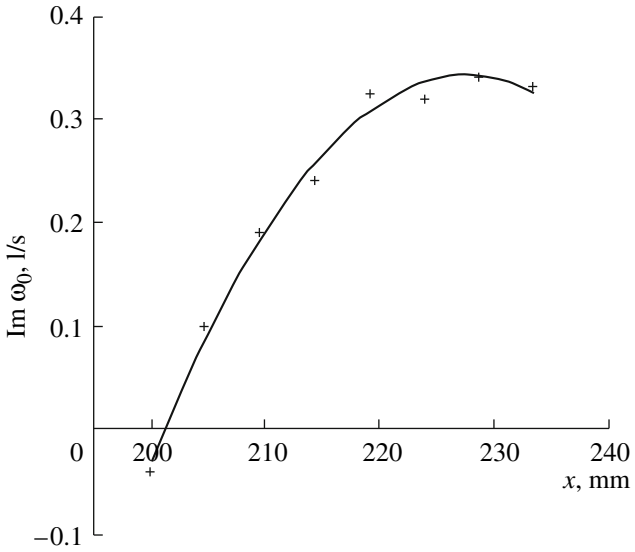

Fig. 12. Area of absolute instability along the direction of jet propagation (the crosses indicate the calculated values of absolute frequencies for different cross sections of the jet, and the solid line indicates the approximation).

frequency $\mathrm{Re}\, f_0$ was marked in the spectrum of oscillations of the upper boundary of the jet (Fig. 9). It can be seen that the theoretical estimates are consistent with observational data.

7. CONCLUSIONS

In a large test reservoir with artificial temperature stratification, we have performed a series of experiments devoted to a major laboratory simulation of the nonstationary dynamics of buoyant turbulent jets (plumes) generated by deepwater sinks from underwater collector diffusers. The interaction of plumes with the pycnocline was found to lead to an active generation of internal waves.

An analysis of the dependence that the wave amplitude has on the control parameter which is proportional to the rate of liquid flow from the collector diffuser, has indicated that this dependence is adequately described by a function that is characteristic for its presence in the Hopf bifurcation system, which occurs for a soft actuation mode of self-oscillations. As is shown in [20], the existence of this dependence is a reliable criterion for the actuation of the globally instable mode.

To check the conditions for the actuation of the globally instable mode, we have performed an auxiliary experiment in a small reservoir with a salt stratification formulated similarly to the experiment in the big reservoir. Using the PIV method, we measured the velocity field in the buoyant jet and constructed the profiles of transverse velocity in several sections. It turned out that, when the jet approaches the pycnocline, a counterflow is generated at the edges. A stability analysis for the resulting profiles of flow velocities performed by the method of normal modes has revealed that, for the jet portions with counterflow, the condition of absolute instability by the Briggs criterion [25] for axisymmetric jet oscillations is satisfied. The presence of absolute instability in a finite interval of the jet testifies to the fact that the globally instable mode is actuated [20]. The estimates for oscillation frequencies of the globally instable mode are well consistent quantitatively with the measured spectrum of jet oscillations. Thus, we can propose the following mechanism for the generation of internal waves by a buoyant jet. When the buoyant jet interacts with the pycnocline, self-oscillations of the globally instable mode appear. If the frequency of these oscillations turns out to be smaller than the maximum buoyancy frequency in the pycnocline, they lead to the active generation of internal waves.

ACKNOWLEDGMENTS

The authors are grateful to Academician A.V. Gaponov-Grekhov, Prof. K.D. Sabinin, and Dr. O.A. Druzhinin for their useful discussions.

REFERENCES

1. V. G. Bondur, "Aerocosmic Methods in Modern Oceanology," in *New Ideas in Oceanology*, Vol. 1: *Physics. Chemistry. Biology* (Nauka, Moscow, 2004), pp. 55–117 [in Russian].
2. V. Bondur, "Complex Satellite Monitoring of Coastal Water Areas," in *31st International Symposium on Remote Sensing of Environment, ISRSE, 2006)* (2006).
3. V. G. Bondur and Yu. V. Grebenyuk, "Remote Indication of Anthropogenic Impacts on the Marine Environment Caused by Deep-Water Sewage Discharge: Modeling and Experiment," Issled. Zemli Kosmosa, No. 6, 1–19 (2001).
4. V. Bondur, R. Keeler, and C. Gibson, "Optical Satellite Imagery Detection of Internal Wave Effects from a Submerged Turbulent Outfall in the Stratified Ocean," GRL **32**, L12610, doi: 10.1029/2005GL022390 (2005).
5. V. G. Bondur, V. M. Zhurbas, and Yu. V. Grebenyuk, "Mathematical Modeling of Turbulent Jets of Deep-Water Sewage Discharge into Coastal Basins," Okeanologiya **46** (6), 805–820 (2006) [Oceanology **46** (6), 757–771 (2006)].
6. V. G. Bondur, V. M. Zhurbas, and Yu. V. Grebenyuk, "Modeling and Experimental Studies of Distribution of Turbulent Jets in the Stratified Medium of Coastal Basins," Okeanologiya **49** (5) (2009) [Oceanology **49** (5), (2009)].
7. C. Y. Koh and H. N. Brooks, "Fluid Mechanics of Waste-Water Disposal in the Ocean," Annu. Rev. Fluid Mech. **8**, 187–211 (1975).
8. J. S. Turner, "Jets and Plumes with Negative or Reversing Buoyancy," J. Fluid Mech. **26**, 779–792 (1966).
9. V. P. Karlikov and O. V. Trushina, "Self-Oscillation of Flat Deep-Water Fountains," Dokl. Akad. Nauk **361** (3), 340–344 (1998).
10. V. P. Karlikov and O. V. Trushina, "Self-Oscillatory Regimes of Flowing of Flat Deep-Water Jets," in *Proceedings of IX All-Russia Congress on Theoretical and Applied Mechanics, Nizhnii Novgorod, 2006* (2006).
11. P. D. Friedman, "Oscillation Height of a Negatively Buoyant Jet," Trans. ASME J: J. Fluids Engng. **128**, 880–882 (2006).
12. P. D. Friedman, V. D. Vadokoot, W. J. Meyer, and S. Carey, "Instability Threshold of a Negatively Buoyant Fountain," Exps. Fluids **42**, 751–759 (2007).
13. N. Williamson, N. Srinarayana, S. W. Armsfield, et al., "Low-Reynolds-Number Fountain Behaviour," J. Fluid Mech. **608**, 297–317 (2008).
14. L. N. Fan, "Turbulent Buoyant Jet Problems," in *Calif. Inst. Technol., W.M. Keck Lab.*, Rep. no. KH-R-18 (1968).
15. V. V. Arabadzhi, S. D. Bogatyrev, V. V. Bakhanov, et al., "Laboratory Modeling of Hydrophysical processes in the Upper Ocean Layer (The Great Thermostratified Basin, Institute of Applied Physics, Russian Academy of Sciences)," in *Near-Surface Ocean Layer. Physical Processes of Remote Probing*, Ed. by V. I. Talanov and E. N. Pelinovskii, (Inst. Prikl. Fiz. Ros. Akad. Nauk, Nizhnii Novgorod, 1999), Vol. 2, pp. 231–251 [in Russian].
16. J. W. Miles, "On the Stability of Heterogeneous Shear Flows," J. Fluid Mech. **10**, 496–508 (1961).

17. L. N. Howard, "Note on a Paper of John W. Miles," J. Fluid Mech. **10**, 509–512 (1961).

18. A. A. Andronov, A. A. Vitt, and S. E. Khaikin, *Vibration Theory* (Nauka, Moscow, 1981) [in Russian].

19. J. T. Stuart, "On the Non-Linear Mechanics of Hydrodynamic Stability," J. Fluid Mech. **4**, 1–21 (1958).

20. P. Huerre and P. A. Monkewitz, "Local and Global Instabilities in Spatially Developing Flows," Annu. Rev. Fluid Mech. **22**, 473–537 (1990).

21. P. A. Monkewitz and K. D. Sohn, "Absolute Instability in Hot Jets and Their Control," AIAA Pap, Nos. 86-1882 (1986).

22. R. J. Adrian, "Particle Imaging Techniques for Experimental Fluid Mechanics," Annu. Rev. Fluid Mech. **23**, 261–304 (1991).

23. P. A. Monkewitz, "The Role of Absolute and Convective Instability in Predicting the Behavior of Fluid Systems," Eur. J. Mech. **9** (5), 395–413 (1990).

24. P. A. Monkewitz, P. Huerre, and J.-M. Chomaz, "Global Linear Stability Analysis of Weakly Non-Parallel Shear Flows," J. Fluid Mech. **251**, 1–20 (1993).

25. R. J. Briggs, *Electron-Stream Interaction with Plasmas* (Mass: MIT Press, Cambridge, 1964).

26. P. A. Monkewitz, "The Absolute and Convective Nature of Instability in Two-Dimensional Wakes at Low Reynolds Numbers," Phys. Fluids **31** (5), 999–1006 (1988).